Theoretical Study of the Output Energy for Various MEMS Based Electrostatic Mechanisms

Ye Mei Lim[1,2], Bin Yang[2], Rama Krishna Kotlanka[2], Chun Huat Heng[1], Jin Xie[2], Min Tang[2], Johnny He Han[2], Hanhua Feng[2], and Chengkuo Lee[1,2,*], *Member, IEEE*

[1] *Department of Electrical and Computer Engineering, National University of Singapore, Singapore 117576*
[2] *Institute of Microelectronics, Agency for Science, Technology and Research (A*STAR), 11 Science Park Rd., Singapore Science Park II, Singapore 117685*

***Abstract* — This paper presents a comparison of the energy harvesting capabilities of 3 different electrostatic mechanisms based on MEMS (Microelectromechanical System) structures which are designed and operated in idea vacuum. The 3 mechanisms that will be compared are the in-plane overlap, in-plane gap closing and out-of-plane gap closing mechanisms. Firstly, it was found that the in-plane gap closing mechanism potentially has the highest output energy amongst the 3 different mechanisms. Secondly, the best energy output for the in-plane gap closing mechanism is approximately 1.8 times that of the out-of-plane gap closing mechanism for load volumes between 5mm^3 and 50mm^3.**

I. Introduction

Traditionally, electronic devices have relied on chemical batteries for power as they are reliable, easily accessible and convenient to use. However, in autonomously operating remote devices where battery replacement is difficult, batteries are not a good solution in the long run. In view of this, researchers have been motivated to harvest energy from the environment to power such remote sensors, with ambient vibrations being one of such energy sources. Since energy harvested from the environment typically produce power in the microwatt range [1], this makes them suitable candidates to power remote sensing applications as these devices have power requirements of the same order [2]. Currently, the 3 means by which energy from vibrations can be harvested are via electrostatic, electromagnetic and piezoelectric mechanisms, and some articles provide a good overview of these techniques [1-3].

Each of these techniques has their own advantages and disadvantages, as well as their respective areas of application [1, 4]. Nonetheless, one common thread which runs through almost all of these works is the aim of increasing the amount of energy that can be harvested from vibrations. In order to improve energy harvesting efficiencies, most traditional vibration energy harvesters operate via the principle of matching their resonant frequencies to the frequency of the target application. However, Külah and Najafi recently has reported an attractive concept in which low frequency vibrations can be harvested by devices having high resonant frequencies [5]. Even though this idea was developed based on an electromagnetic mechanism, the concept can be extended to other energy conversion schemes.

*Corresponding author. Tel.: +65 65165865; E-mail: elelc@nus.edu.sg

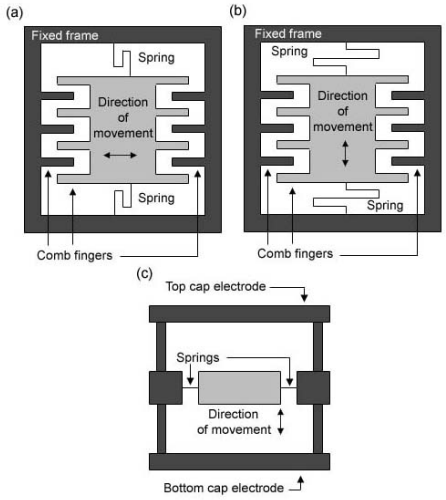

Fig. 1 The 3 different electrostatic mechanisms. The dark areas represent the fixed elements and the light areas, the movable elements. (a) In-plane overlap converter. (b) In-plane gap closing converter. (c) Out-of-plane gap closing converter.

Theoretically, it was found that the electrostatic mechanism has the lowest energy harvesting capabilities amongst all the 3 mechanisms [2]. However, despite this, electrostatic transducers do have specific advantages and area of application. Firstly, electrostatic devices use mainly silicon as the device structural material. Secondly, it facilitates CMOS integration.

Due to limited research works which have been reported for the electrostatic harvesting mechanisms, the intention of this paper is to study how device configurations can affect the energy output so as to find the best mechanism in general. Thus, a methodology is presented to compare the energy harvesting capabilities of 3 major electrostatic mechanisms (i.e. in-plane overlap, in-plane gap closing and out-of-plane gap closing mechanisms) as depicted in Fig. 1. Since the methodology developed for this comparison is based on comparing the energy output per energy harvesting cycle of the device, the results are generic and it can be applied to both the traditional conversion scheme (in which the resonant frequency of the device is matched to the application) as well as the frequency up-conversion scheme developed by Külah and Najafi [5]. Besides, in this study, the indicator of output energy density will be obtained by normalizing the output energy with the devices' active volume as it provides a fair basis for comparison between different

978-1-4244-1888-6/08/$25.00 ©

mechanisms.

II. THEORETICAL BACKGROUND

For all the 3 mechanisms illustrated in Fig. 1, the capacitances of these structures exhibit the minimum value at devices' rest position, i.e., the central position, and become the maximum value corresponding to the maximum displacement in each vibration cycle. However, what distinguishes the 3 mechanisms from each other is the manner in which this varying capacitance is achieved. The in-plane overlap converter varies the overlap area between electrode fingers, the in-plane gap closing converter varies the gap between electrode fingers, and the out-of-plane gap closing converter varies the gap between two large electrode plates.

Typically, there are two methods in which the energy conversion can occur based on electrostatic mechanisms, and they are namely the voltage-constrained and charge-constrained conversion methods. With reference to this, a paper by Torres and Rincón-Mora has presented some of the energy losses associated with a voltage-constrained scheme [6]. However, in most of the research which has been done, the charge-constrained method is more popular over the voltage-constrained method as it requires just one external charge reservoir instead of two. For this reason, the discussion will just be focused on the charge-constrained method. For the purposes of describing how the energy harvesting process works, a movable parallel plate capacitor will be assumed in the explanation of the charge-constrained conversion cycle.

When the structure is vibrated, the energy conversion cycle begins when the capacitance of the structure momentarily reaches a maximum value of C_{max}. At this point, an external charge reservoir deposits a charge across the electrodes and a potential difference of V_{start} can be measured across the electrodes. This charging process is represented by the path from point A to point B in Fig. 2 [3].

After the variable capacitor has been charged to V_{start}, the electrodes are electrically isolated and the physical separation between the electrode plates is forced to increase. This is the actual step in which mechanical energy is being converted to electrical energy, and it is represented in Fig. 2 as the path from point B to C. During this phase, the charges on the plates are forced to remain constant, the capacitance of the device decreases to a minimum C_{min}, and the potential difference across the device increases to a maximum V_{max}. Finally, when the variable capacitor has reached its minimum value, C_{min}, the charge on the capacitor is discharged back into the charge reservoir. This is represented by the path from point C to point A, and it concludes one energy conversion cycle.

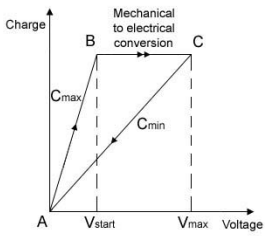

Fig. 2 A charge-constrained conversion cycle

Typically, a parallel capacitor, C_{par}, will be connected in parallel to the MEMS capacitor to limit the maximum voltage that is reached by the system. This is required in practice because circuits are only able to tolerate voltages below a certain limit, above which the switches in the circuit will break down. With the addition of such a parallel capacitor, the following energy equations will be in force

$$V_{\max} = \frac{C_{\max} + C_{par}}{C_{\min} + C_{par}} V_{start} \quad (1)$$

$$E_{conv} = \frac{1}{2} V_{start}{}^2 \frac{C_{\max} + C_{par}}{C_{\min} + C_{par}} (C_{\max} - C_{\min}) \quad (2)$$

$$= \frac{1}{2} V_{start} V_{\max} (C_{\max} - C_{\min}) \quad (3)$$

where E_{conv} is the amount of energy converted from mechanical to electrical in one conversion cycle.

III. OPERATION MECHANISM AND MODELLING APPROACH

In order to determine the mechanism with the best energy output density, specific design topologies were developed for each of these cases, and they are illustrated in Fig. 3 and Fig. 4. Each of these structures consists of movable as well as fixed components, and they have been labeled respectively in Fig. 3 and 4. In addition, the regions which have been highlighted with dotted lines in the figures are the volumes that the output energy will be normalized against. These volumes are chosen because it is mainly within these defined active regions that the energy conversion is taking place. In addition, all of these structures are assumed to have a 0.1μm silicon nitride (Si_3N_4) dielectric coating to allow the electrodes to come into contact with each other during normal device operation and hence increase the devices' energy output. As a matter of fact, we assume all these 3 mechanisms operate in ideal vacuum environment. Thus we can achieve C_{max} by having two electrodes contact with each other.

With reference to Fig. 4, the presence of the electrical isolation in the middle of the movable centre mass in the out-of-plane gap closing structure allows for two energy

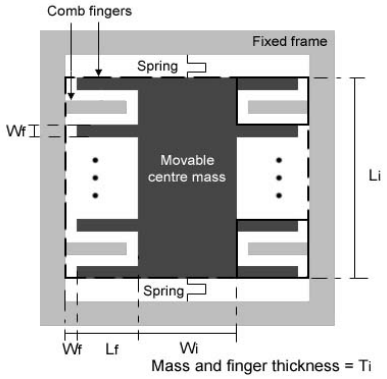

Fig. 3 Top view of the in-plane overlap and in-plane gap closing structure

conversion cycles in one mechanical oscillation. This is made possible because there are two separate sets of capacitor plates in such a structure, with the first being that of the fixed top cap electrode with the top half of the movable centre mass, and the second set being that of the fixed bottom cap electrode with the bottom half of the movable centre mass. Hence, this increases the output power of the device. This idea of introducing an electrical isolation in the middle of an electrode plate is a novel conception.

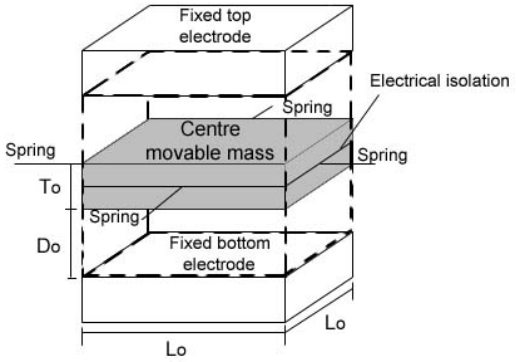

Fig. 4 Side view of the out-of-plane gap closing structure

If the in-plane overlap and in-plane gap closing converters were to be compared, it can be observed that the C_{max} of the in-plane overlap converter is very similar in magnitude to the C_{min} of the in-plane gap closing structure. For example, by considering sample comb finger dimensions from the work done by Chui et al. [7], the C_{max} for one set of combs for the in-plane overlap converter will be 0.122pF, and the C_{min} can be treated to be zero. On the other hand, for the same comb finger dimensions, the C_{max} will be 0.149nF and the C_{min} will be 0.122pF for one comb set in the in-plane gap closing converter. By referring to equation 3, it is observed that the in-plane gap closing generator would have an output that is of the order of 1000 times that of the in-plane overlap generator. Since these two generators have similar geometries for similar structural dimensions, it can be concluded from this comparison that the energy output density for the in-plane overlap generator is very much less than that of the in-plane gap closing mechanism. Hence, the focus of this paper can just be on comparing the energy output density between the in-plane gap closing and out-of-plane gap closing mechanisms.

Firstly, in the simulation, the mass of the movable load in both the in-plane gap closing and out-of-plane gap closing structures is set to be equal. This is to allow for their resonant frequencies to be similar, assuming that they have the same effective spring constants. On the other hand, we assume all these devices are packaged and tested in idea vacuum. Thus we do not include the consideration of air damping effect versus different mechanisms. Additionally, if the two structures have the same operating frequencies, it simplifies the comparison between the power outputs as just the energy output per harvesting cycle can be compared to compare the power output.

The other parameter that will be kept constant between the two devices is the cross sectional area of their active regions. For simplicity, these cross sectional areas would also be assumed to have their lengths equal to their widths.

Lastly, to simplify the mathematical model, we assume that the numerical value of the comb fingers' width is equivalent to the gap between adjacent comb fingers.

For the first constraint in which the movable loads are set to have equal masses, and taking the aspect ratio to be a reasonably practical value of 20:1, the following equation can be derived

$$L_o{}^2 T_o = W_i L_i T_i + \frac{20L_i - T_i}{40} L_f T_i \tag{4}$$

where the parameters mentioned in the equation are graphically defined in Fig. 3 and Fig. 4.

For the second constraint in which the cross sectional area of the active regions for the two structures have the same dimensions, and referring to Fig. 3 and Fig. 4, there are the equations

$$L_i = L_o \tag{5}$$

$$2L_f + W_i + 2\frac{T_i}{20} = L_i \tag{6}$$

Combining these equations, the comb finger length and the width of the central mass in the in-plane gap closing structure can be written as such

$$L_f = \frac{40L_i{}^2 T_i - 40L_o{}^2 T_o - 4L_i T_i{}^2}{T_i{}^2 + 60L_i T_i} \tag{7}$$

$$W_i = L_i - \frac{80L_i{}^2 T_i - 80L_o{}^2 T_o - 8L_i T_i{}^2}{T_i{}^2 + 60L_i T_i} - \frac{T_i}{10} \tag{8}$$

For the purposes of defining the active device volume which will be considered in the normalization of energy later, an additional constraint is set up to equate the displacement of the mass in the out-of-plane gap closing mechanism to that of the mass in the in-plane gap closing mechanism. This implies that the amplitude of vibration of the movable loads in both mechanisms is set to be the same. With reference to Fig. 3 and Fig. 4, as well as the consideration of the aspect ratio of 20:1, the following equality can thus be obtained

$$D_o = \frac{T_i}{20} \tag{9}$$

The design of the out-of-plane gap closing structure is relatively straightforward, given that the cross sectional area of the active region and the mass of the movable load are fixed. However, for the in-plane gap closing mechanism, there can be many combinations of different dimensional parameters for the same active area and load mass. In particular, the effects of varying the thickness of the mass in the in-plane structure on the C_{max}, C_{min} and energy output of the in-plane gap closing structure will be studied.

IV. RESULTS AND DISCUSSION

In each of the curves in Fig. 5, the C_{max} for the in-plane gap closing structure is plotted against T_i, whilst keeping the cross sectional area of the active region constant at 1cm^2 and the volume (and hence mass) of its movable load at a certain constant value. Additionally, different

curves are plotted for loads of different volumes (and hence masses). The rationale behind choosing the minimum and maximum load volumes as $5mm^3$ and $50mm^3$ respectively stems from practical fabrication considerations. For a volume of $5mm^3$, the out-of-plane structure's mass thickness would be 50µm. By considering that the cross sectional area of the mass is $1cm^2$, this value presents the lower realizable limit for the mass thickness owing to practical fabrication considerations. On the other hand, for a volume of $50mm^3$ and a cross sectional area of $1cm^2$, the thickness of the out-of-plane movable mass would be 500µm. This thickness is almost equivalent to the thickness of a typical wafer, and we thus treat it to be the upper limit for the mass thickness. Hence, for a cross sectional area of $1cm^2$, the volumes of $5mm^3$ and $50mm^3$ presents the upper and lower limits respectively for the purposes of our comparison, with all other volumes within these 2 extremes forming the spectrum of typical mass volumes.

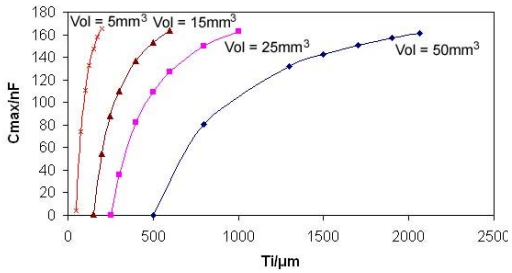

Fig.5 Graph of C_{max} (for the in-plane gap closing mechanism) against the thickness of the mass in the in-plane gap closing structure for load masses with different volumes

During the computation of the parameters, it was observed that within each curve (in Fig. 5), T_i can only assume values within a specific range, as values beyond this range it would result in the finger length or the mass width undertaking negative values and being unrealistic. Hence, within each curve, the energy output is being plotted against the entire range of plausible T_i accordingly. From Fig. 5, it can be seen that the C_{max} for each of the different loads is approximately the same, and they all occur at the maximum T_i value within each curve. Similarly, the C_{min} for the in-plane gap closing structure is also plotted against Ti in Fig. 6. By comparing Fig. 5 and Fig. 6, it is observed that the C_{max} is of the order of about 100 times that of the C_{min}.

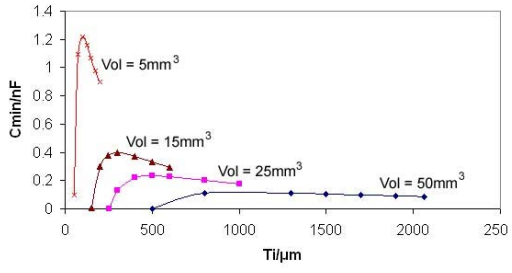

Fig.6 Graph of C_{min} (for the in-plane gap closing mechanism) against the thickness of the mass in the in-plane gap closing structure for load

The energy output optimization process can be demonstrated by selecting one set of C_{max} and C_{min}. For illustration purposes, the point at which C_{max} is at its maximum for the case where Vol = $25mm^3$ will be selected. At this particular point, C_{max} is 162.8nF and C_{min} is 0.174nF. The 3D graph of V_{max} against C_{par} and V_{start} as well as the 3D graph of energy output against C_{par} and V_{start} are then plotted in Fig. 7 and Fig. 8 respectively in the following ranges

$$0.1C_{\max} \le C_{par} \le 2C_{\max}$$

$$0 \le V_{start} \le 5V$$

There ranges are selected by taking into consideration practical circuit constraints, which typically limit the V_{start} to be below 5V and the V_{max} to be below 20V.

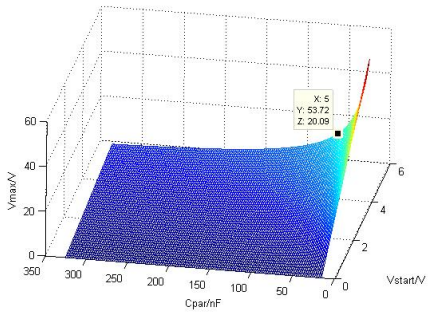

Fig. 7 3D Graph of V_{max} against C_{par} and V_{start} for the in-plane gap closing structure (C_{max} = 162.8nF, C_{min} = 0.174nF)

In Fig. 8, it is observed that the energy output increases with decreasing C_{par} and increasing V_{start} for any given fixed C_{max} and C_{min}. Hence, it makes sense to set V_{start} to be of the limit of 5V and consider the optimum value of C_{par} which would give the maximum realizable V_{max} of 20V. The corresponding energy output would hence be the maximum possible output after taking into consideration all the above voltage constraints. In this particular case considered, a C_{par} of 54nF would give a V_{max} of 20V and an energy output per cycle of 8.2µJ for a V_{start} of 5V. The above steps are repeated for all the other pairs of points in the graphs in Fig. 5 and 6, and the optimum energy output for the in-plane gap closing structure for different mass values is presented in Fig. 9.

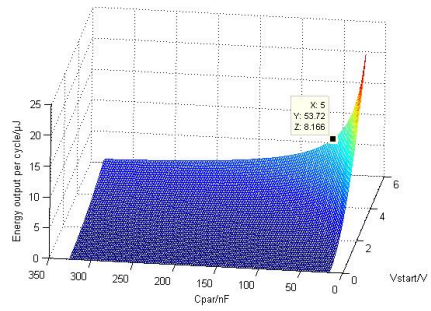

Fig. 8 3D Graph of energy output per cycle against C_{par} and V_{start} for the in-plane gap closing structure (C_{max} = 162.8nF, C_{min} = 0.174nF)

Next, for different load volumes, the energy outputs that are normalized against the structures' active volumes for both the in-plane and out-of-plane gap closing mechanisms are plotted against T_i and the loads' maximum displacement in Fig. 10. This displacement parameter is crucial in determining the active device volume for the out-of-plane gap closing structure as can be seen from Fig. 4, and is hence included in the graphs in Fig. 10. It is observed in all 4 cases that if the thickness of the mass in the in-plane gap closing structure is greater than a certain critical thickness, the energy output density for the in-plane gap closing mechanism is greater than the out-of-plane gap closing mechanism. Additionally, for each of the cases presented, there is an optimum value for the mass thickness in the in-plane structure for which the energy output density of the in-plane gap closing mechanism peaks at a maximum possible value.

In relation to this, the best energy output density for both the in-plane gap closing and out-of-plane gap closing mechanism for each load volume can be deduced and plotted for various load volumes in a graph like that in Fig. 11. Referring to this graph, it is observed that the best energy output density for the in-plane gap closing mechanism is always higher than that of the out-of-plane gap closing mechanism for all load volumes between $5mm^3$ and $50mm^3$. Additionally, the ratio of the best energy output for the in-plane gap closing mechanism to the out-of-plane gap closing mechanism is approximately consistent at 1.8 for load volumes between $5mm^3$ and $50mm^3$.

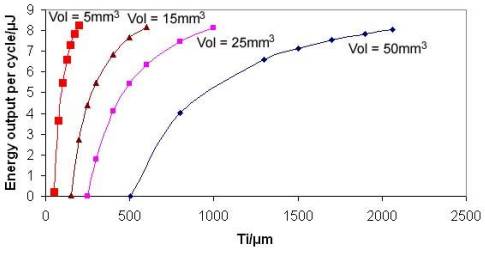

Fig.9 Graph of energy output per cycle (for the in-plane gap closing mechanism) against the thickness of the mass in the in-plane gap closing structure for load masses with different volumes

V. CONCLUSION

The focus of this paper is to present a systematic method to compare the energy harvesting capabilities of the 3 electrostatic mechanisms. This analytical method allows future researchers to have a basis to select the appropriate MEMS mechanism in the design of similar designs in order to maximize the energy output. For the few cases looked into, it is observed that the in-plane gap closing mechanism has the potential to produce a higher amount of energy per unit volume as compared to the out-of-plane gap closing mechanism in vacuum. Additionally, the best energy output for the in-plane gap closing mechanism is approximately 1.8 times that of the out-of-plane gap closing mechanism for load volumes between $5mm^3$ and $50mm^3$. Even though this paper has only considered the cases in which the load masses have volumes between $5mm^3$ and $50mm^3$, it is expected that the trends observed will also be reflected in cases with mass volumes beyond this range, and the results can thus be extrapolated to various cases under the same scenario. This hence provides more insight into the energy harvesting capabilities of each technique.

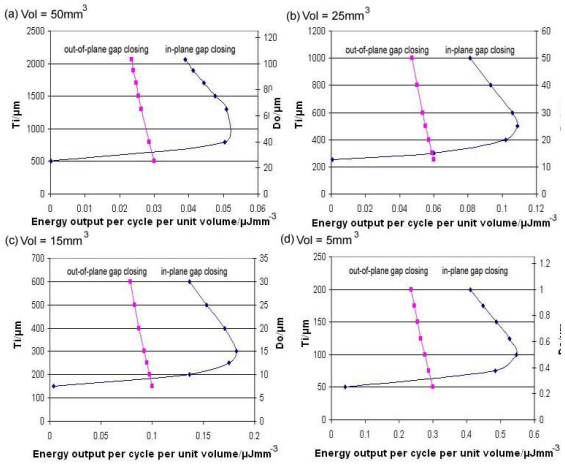

Fig. 10 Graphs of the energy output densities plotted against the thickness of the mass in the in-plane gap closing structure and the maximum mass displacements, where the load has a volume of (a) $50mm^3$, (b) $25mm^3$, (c)$15mm^3$, and (d) $5mm^3$.

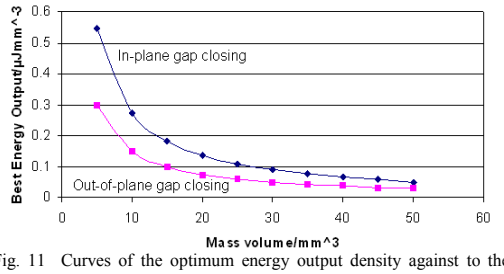

Fig. 11 Curves of the optimum energy output density against to the volume of movable mass.

ACKNOWLEDGEMENT

This research work was partially supported by grants from A*STAR HOME 2015 National Research Programme (SERC grant number: 0621150043) and a joint-funded research project R-263-000-358-112/133 of the National University of Singapore and the Institute of Microelectronics, A-STAR, Singapore.

REFERENCES

[1] S. P. Beeby, M. J. Tudor, N. M. White, "Energy harvesting vibration sources for microsystems applications," *Meas. Sci. and Technol.,* vol. 17, pp.175-195, 2006.

[2] S. Roundy, P. K. Wright, and J. Rabaey, "A study of low level vibrations as a power source for wireless sensor nodes," *Computer Communications,* vol. 26, pp. 1131-44, 2003.

[3] S. Meninger, J. Mur-Miranda, R. Amirtharajah, A. Chandrakasan, and J. Lang, "Vibration-to-electric energy conversion," IEEE Trans. on Very Large Scale Integration (VLSI) Systems, vol. 9, pp. 64-76, 2001.

[4] P. Miao, P. D. Mitcheson, A. S. Holmes, E. M. Yeatman, T. C. Green, and B. H. Stark, "MEMS inertial power generators for biomedical applications," *Microsyst. Technol.,* vol.12, pp.1079-1083, 2006.

[5] H. Külah and K. Najafi, "Energy scavenging from low-frequency vibrations by using frequency up-conversion for

wireless sensor applications," *IEEE Sensors Journal,* vol. 8, pp. 261-268, 2008.

[6] E. O. Torres and G. A. Rincón-Mora, "Electrostatic energy harvester and li-ion charger circuit for micro-scale applications," *Proc. of the 49th IEEE International Midwest Symposium on Circuits and Systems*, pp. 65-69, 2006.